

This is an Open Access document downloaded from ORCA, Cardiff University's institutional repository:<https://orca.cardiff.ac.uk/id/eprint/122860/>

This is the author's version of a work that was submitted to / accepted for publication.

Citation for final published version:

Mokhti, Zulhazmi A., Lees, Jonathan , Cassan, Cedric, Alt, Alexander and Tasker, Paul J. 2019. The nonlinear drain-source capacitance effect on continuous-mode class-B/J power amplifiers. *IEEE Transactions on Microwave Theory and Techniques* 67 (7) , pp. 2741-2747. 10.1109/TMTT.2019.2918309

Publishers page: <http://dx.doi.org/10.1109/TMTT.2019.2918309>

Please note:

Changes made as a result of publishing processes such as copy-editing, formatting and page numbers may not be reflected in this version. For the definitive version of this publication, please refer to the published source. You are advised to consult the publisher's version if you wish to cite this paper.

This version is being made available in accordance with publisher policies. See <http://orca.cf.ac.uk/policies.html> for usage policies. Copyright and moral rights for publications made available in ORCA are retained by the copyright holders.



# The Nonlinear Drain-Source Capacitance Effect on Continuous Mode Class-B/J Power Amplifiers

Zulhazmi Mokhti, *Member, IEEE*, Jonathan Lees, *Member, IEEE*, Cedric Cassan, *Member, IEEE*, Alexander Alt, *Student Member, IEEE*, and Paul J. Tasker, *Fellow, IEEE*

**Abstract**—The effects of the nonlinear drain-to-source capacitance ( $C_{DS}$ ), or the varactor effect, on the operation of continuous mode class-B/J power amplifiers are described in terms of mathematical analysis as well as experimental validation. The nonlinear  $C_{DS}$  generates harmonic current when the class-B/J drain voltage is applied across it, modifying the theoretical load trajectories on the Smith Chart. This is shown to significantly deviate from the continuous mode assertion of constant power and efficiency. A novel measurement approach called *voltage-pull* is used to investigate the effects of the 2<sup>nd</sup> harmonic generation by the varactor in a class-B/J power amplifier mode. Theoretical and experimental results showed the nonlinear  $C_{DS}$  degrades the drain efficiency compared to class-B on one half of the class-B/J design space while improving the other half due to the energy up and down-conversion, respectively. This work provides an approach for die nonlinear characteristic optimizations for transistor manufacturers.

**Index Terms**— Class B, class J, continuous mode, drain-to-source capacitance, load-pull, non-linear output capacitance, power amplifiers, varactor, voltage pull.

## I. INTRODUCTION

THE CONCEPT of extending the design space of a high-efficiency mode power amplifier (PA) was first introduced by Cripps in [1]. In that work, a new design space was presented identifying a continuum between class-B and class-J, enabling a design that maintains a class-B performance in terms of power and efficiency, and that as a result paves the way for high-efficiency mode design over considerable bandwidth. In [2] the continuous mode theory was applied to class-F validating a new design space using an active load-pull measurement setup that led to the realization of a continuous class-F PA in [3] which produced a class-F type efficiency of 74% over an octave bandwidth using a 10W GaN device.

The formulation of continuous class-B/J voltage waveforms in [1] assumes an ideal half-rectified current waveform.

Manuscript received Jul 23, 2018, revised Apr 17, 2019. This work was supported by NXP Toulouse, France, Cardiff University Center of High Frequency Engineering, UK, Cree Morgan Hill, CA, USA and the Engineering and Physical Science Research Council (EPSRC) in the context of the research project EP/N016408/1.

Z. Mokhti was with Cardiff University, UK. He is now with Cree's Wolfspeed division in Morgan Hill, CA, USA (email: [zmokhti@cree.com](mailto:zmokhti@cree.com)).

However, in a real device, the presence of the drain-to-source capacitance ( $C_{DS}$ ) whose value changes nonlinearly with drain voltage and in a way that is specific to the device technology, introduces harmonic current and changes the nature of the current delivered to the load. This results in the change of the effective fundamental and harmonic loads seen by the current generator plane.

This paper aims to provide a mathematical explanation of the varactor effect on continuous class-B/J power amplifiers when the output voltage adheres to the continuous class-B/J voltage definition. The nonlinear  $C_{DS}$  generates 2<sup>nd</sup> harmonic current, and the termination selection can cause the current generator plane to see a 2<sup>nd</sup> harmonic ‘injection’ effect, which is similar to the effect investigated in [4]-[8] to improve PA efficiency. An analysis to isolate the contribution of the nonlinear  $C_{DS}$  alone on efficiency is first explored, followed by an experimental validation using an active load-pull system.

## II. CONTINUOUS CLASS-B/J POWER AMPLIFIER THEORY

The basis of the continuous class-B/J power amplifier starts with the formulation of the class-J power amplifier that was introduced in [9]. The class-J PA applies a phase shift on the fundamental and 2<sup>nd</sup> harmonic loads of a class-B mode PA at -45° and 90°, respectively and retains the class-B output power and efficiency performance.

The continuous class-B/J PA applies a raised sine function of the continuous mode operator  $(1 - \alpha \sin \vartheta)$  to the normalized class-B output voltage,

$$v_{BJ}(\vartheta) = V_{max}(1 - \cos \vartheta) \cdot (1 - \alpha \sin \vartheta) \quad (1)$$

where the range of  $\alpha$  is defined from -1 to 1 to keep the voltage above zero. With the current waveform kept as a half-rectified cosine wave, see equation (2), the variation of  $\alpha$  creates a continuum of design space in the fundamental and 2<sup>nd</sup> harmonic load termination pairs.

J. Lees, A. Alt, and P. Tasker are with Cardiff University Center of High Frequency Engineering, CF24 3AA, Wales, UK (email: [LeesJ2@cardiff.ac.uk](mailto:LeesJ2@cardiff.ac.uk); [AltA@cardiff.ac.uk](mailto:AltA@cardiff.ac.uk); [tasker@cardiff.ac.uk](mailto:tasker@cardiff.ac.uk)).

C. Cassan is with NXP Semiconductors, 31100 Toulouse, France (e-mail: [cedric.cassan@nxp.com](mailto:cedric.cassan@nxp.com)).

$$i_{BJ}(\vartheta) = I_{max} \cos \vartheta \quad 0 < \vartheta < \frac{\pi}{2}, \frac{3\pi}{2} < \vartheta < 2\pi$$

$$= 0 \quad \frac{\pi}{2} < \vartheta < \frac{3\pi}{2}$$
(2)

Fig. 1 shows the ideal class-B/J output voltage and current waveforms as well as the fundamental and 2<sup>nd</sup> harmonic load trajectories as  $\alpha$  is varied from -1 to 1 in 0.2 steps.

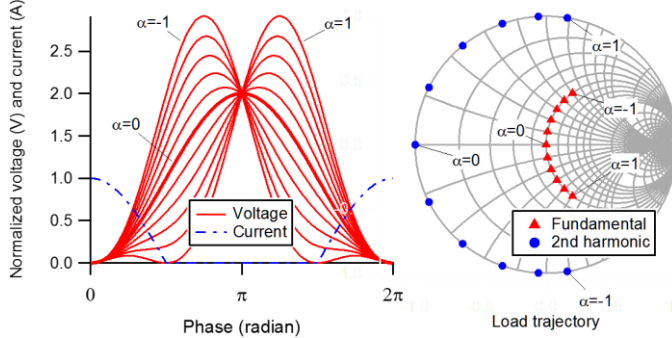


Fig. 1. Class-BJ ideal output voltage and current waveforms (left), and ideal load trajectory (right) at the current generator plane.

### III. MATHEMATICAL ANALYSIS OF THE NONLINEAR $C_{DS}$ EFFECT ON CLASS-B/J POWER AMPLIFIERS

#### A. Applying the Varactor Effect in Class-B/J Mode

Fig. 2 shows a simplified equivalent circuit of a transistor with a lossless nonlinear  $C_{DS}$  operating in an otherwise ideal continuous class-B/J mode. The  $C_{DS}$  produces fundamental and harmonic current depending on the voltage across it which is defined in (1). A linear de-embedding approach is applied where a negative capacitor  $C_{fixed}$  is used to counteract the  $C_{DS}$  effect at the reference class-B ( $\alpha=0$ ) operating condition. However, the linear de-embedding approach does not cancel out  $C_{DS}$  completely, leaving a residual displacement current which is dependent on  $\alpha$ .

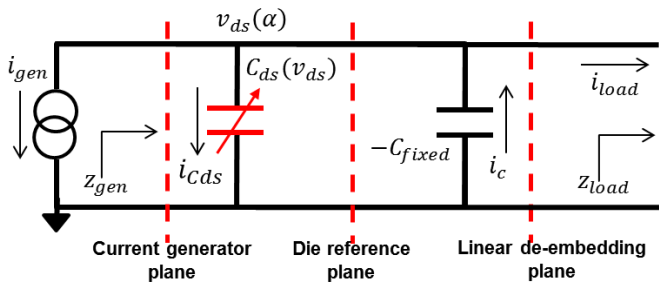


Fig. 2. Simplified circuit diagram of the device with a nonlinear  $C_{DS}$  de-embedded with a fixed negative capacitor.

Assuming negligible series inductance, the load current is given by:

$$i_{load}(\alpha) = -i_{gen} - \frac{dv_{ds}(\alpha)}{dt} [C_{ds}(v_{ds}) - C_{fixed}] \quad (3)$$

A typical  $C_{DS}$  behavior can be modelled by the equation:

$$C_{ds}(v_{ds}) = C_{offset} + \frac{C_0}{(1 + v_{ds}/v_0)^m} \quad (4)$$

where  $C_{offset}$ ,  $C_0$ ,  $v_0$ , and  $m$  are fitting parameters. To proceed with this analysis, a nonlinear  $C_{DS}$  based on the NXP LDMOS 50V device is used ( $C_{offset}=0.8$  pF,  $C_0=5.5$  pF,  $v_0=11$  V, and  $m=2$ ), in an otherwise ideal class-B/J mode power amplifier settings in Table I. Applying (4) into (3) the time-domain voltage and current waveforms as a function of  $\alpha$  at the linear de-embedding plane (LDP) are shown in Fig. 3. The selection of  $C_{fixed}$  value, in this case 1.19 pF, serves to shift the fundamental load to the real axis on the linear de-embedding plane but does not affect output power and efficiency.

Using FFT, fundamental and 2<sup>nd</sup> harmonic load trajectories of continuous class-B/J mode at the current generator and linear de-embedding planes were calculated for  $-1 \leq \alpha \leq 1$  in 0.1 steps, as shown in Fig. 4. The 2<sup>nd</sup> harmonic load trajectory goes inside the Smith chart for  $-1 < \alpha < 0$  indicating a resistive load requirement and consequential power dissipation, while for  $0 < \alpha < 1$  the 2<sup>nd</sup> harmonic load appears outside the Smith chart indicating a 2<sup>nd</sup> harmonic ‘injection’ is required at the die plane to maintain the class-B/J voltage waveforms.

TABLE I  
DEVICE PARAMETERS AND OPERATING CONDITIONS

Operating drain dc voltage	50 V
Maximum drain current	0.8 A
Knee voltage	0 V
Conduction angle	180 (Class-B bias)
Fundamental frequency	900 MHz

Only at  $\alpha=0$  is the original class-B/J 2<sup>nd</sup> harmonic load condition maintained, while at the extreme  $\alpha$  values of -1 and 1, the 2<sup>nd</sup> harmonic load is located on the edge of the Smith chart, although with a phase offset from the ideal case. With the linear de-embedding, the change in the fundamental load trajectory is negligible in this example.

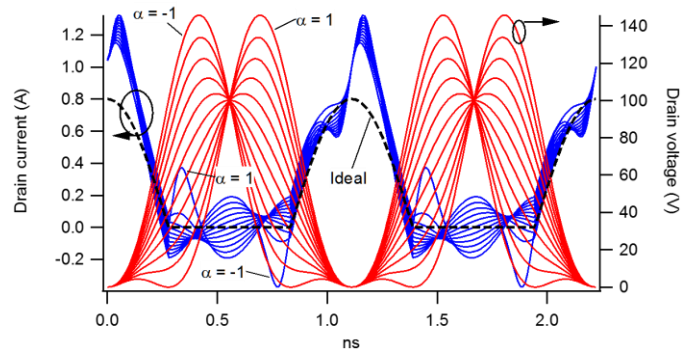


Fig. 3. Calculated time domain voltage (red) and current (blue) waveforms at the linear de-embedding plane for  $-1 < \alpha < 1$  in 0.2 steps.

The modification of the load trajectories tallies with the calculated fundamental and 2<sup>nd</sup> harmonic output power trend as

a function of  $\alpha$ , as shown in Fig. 5. For  $-1 < \alpha < 0$  as the 2<sup>nd</sup> harmonic load enters the Smith chart, the 2<sup>nd</sup> harmonic output power increases while the fundamental power drops by the same amount, indicating an energy up-conversion. Consequently, the calculated drain efficiency also drops compared to the ideal class-B/J efficiency for this range of  $\alpha$ .

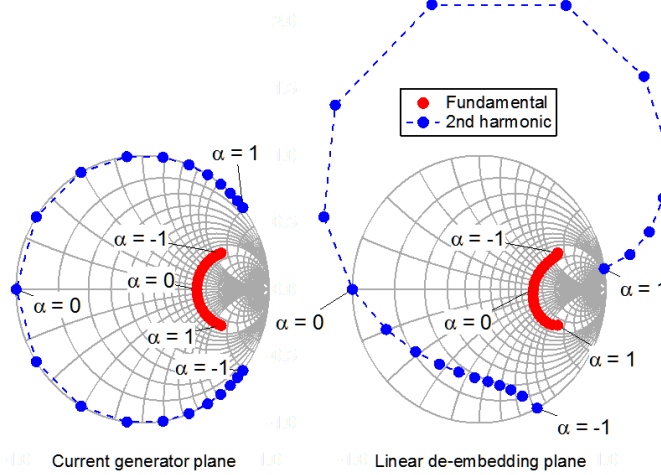


Fig. 4. Calculated class-B/J fundamental (red) and 2<sup>nd</sup> harmonic (blue) loads at the current generator plane (left) and the linear de-embedding plane as a function of  $\alpha$  with the nonlinear  $C_{DS}$  effect.

Conversely and importantly, for  $0 < \alpha < 1$ , where the 2<sup>nd</sup> harmonic load sits outside the Smith chart, energy down-conversion is observed from 2<sup>nd</sup> harmonic to the fundamental, causing the fundamental power to increase in line with the injected 2<sup>nd</sup> harmonic power. For this  $\alpha$  range, an interesting observation is that the drain efficiency has increased to a maximum of 85 % compared to the ideal class-B/J efficiency of 78.6 % due to the required 2<sup>nd</sup> harmonic injection at the load to maintain the class-B/J voltage waveforms. The change in fundamental output power is as high as  $\pm 8\%$  and the delta in drain efficiency is  $\pm 6.5\%$ -point.

#### B. Shifting the 2<sup>nd</sup> Harmonic Load to the Edge of Smith Chart

It is desirable to shift the 2<sup>nd</sup> harmonic loads on the linear de-embedding plane to the edge of the Smith chart to enable a passive load implementation, especially in the case of positive  $\alpha$  range values. For the negative  $\alpha$  values, pushing the 2<sup>nd</sup> harmonic loads from inside the Smith chart towards the edge presents a high-reflect to the 2<sup>nd</sup> harmonic component, thus preventing the energy conversion from the fundamental frequency to 2<sup>nd</sup> harmonic as was originally observed in Fig. 5.

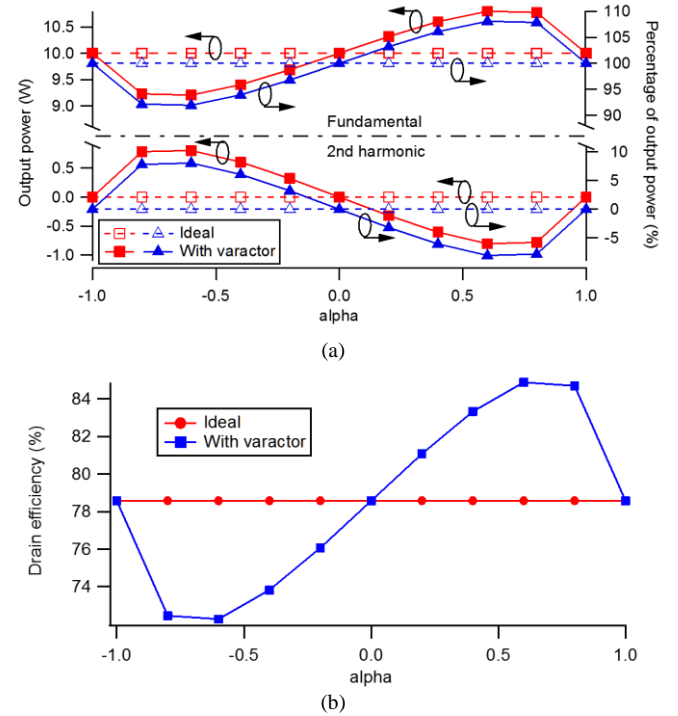


Fig. 5. Calculated fundamental and 2<sup>nd</sup> harmonic power with and without the varactor effect (a) and the resulting drain efficiency (b).

Moving the 2<sup>nd</sup> harmonic loads is done by applying a phase shift term  $\varphi$  for each  $\alpha$  in the continuous class-B/J time-domain output voltage, which changes the fundamental and 2<sup>nd</sup> harmonic loads simultaneously:

$$v_{ds}(\alpha) = V_{max}(1 - \cos(\theta + \varphi))(1 - \alpha \sin(\theta + \varphi)) \quad (5)$$

An iterative search of the phase shift value  $\varphi$  is done for each value of  $\alpha$  until the 2<sup>nd</sup> harmonic load is located on the edge of the Smith chart (reflection coefficient of 1). No phase shift is needed at  $\alpha=1$  and  $\alpha=-1$ , since the 2<sup>nd</sup> harmonic loads are already located on the edge of the Smith chart. As for  $\alpha=0$ , an interpolated phase shift is applied to maintain the continuity of the fundamental load trajectory. Fig. 6 shows the required phase shift amount calculated for each  $\alpha$  for the previous example.

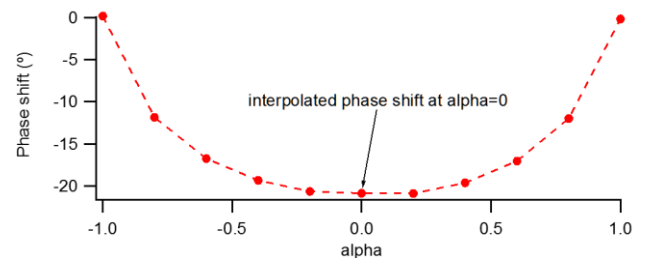


Fig. 6. Required phase shift to bring the 2<sup>nd</sup> harmonic load to the edge of the Smith chart.

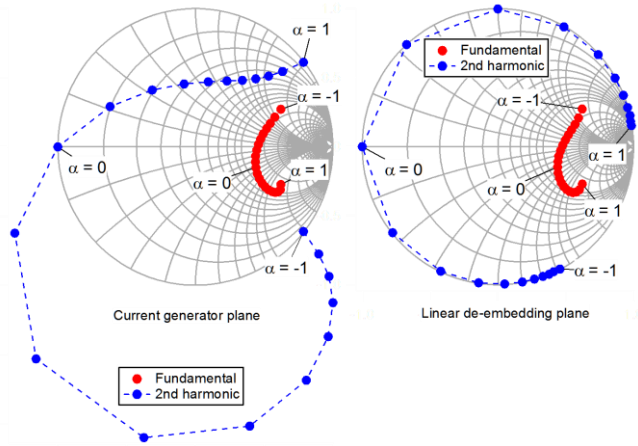


Fig. 7. Calculated fundamental and 2<sup>nd</sup> harmonic load trajectories after phase shift, at the current generator (left) and linear de-embedding planes (right).

The resulting fundamental and 2<sup>nd</sup> harmonic load trajectories after the phase shift is applied are shown in Fig. 7. With a passive termination applied on the load (represented by the linear de-embedding plane), the current generator plane now sees a 2<sup>nd</sup> harmonic injection effect for negative  $\alpha$  values.

The phase-shifting counteracts the energy conversion phenomenon between fundamental and 2<sup>nd</sup> harmonic for all  $\alpha$ . The output power is now kept at the fundamental frequency only, and the 2<sup>nd</sup> harmonic power is removed at the linear de-embedding plane, as shown in Fig. 8.

This also results in a change in drain efficiency, as shown in Fig. 9. For positive  $\alpha$  values, the calculated efficiency drops since the 2<sup>nd</sup> harmonic injection effect has been removed with the loads now relocated to the edge of the Smith chart. At  $\alpha=0$ , the efficiency drops from the ideal class-B number of 78.6% to 73%, as the fundamental load is shifted from the optimum location on the real axis of the Smith chart to an interpolated reactive load to allow for a continuous design space.

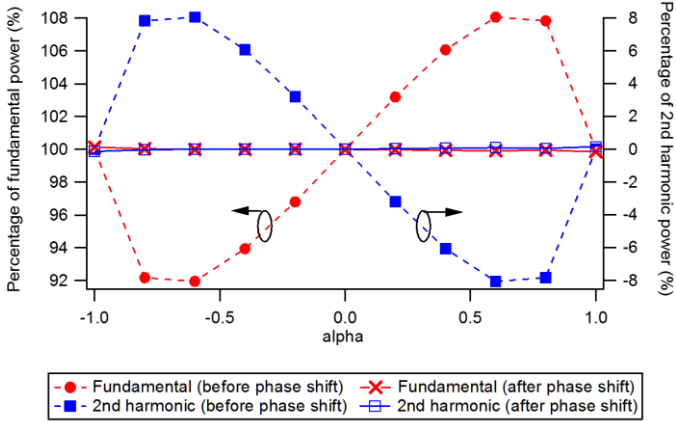


Fig. 8. Calculated output power distribution before and after phase shift.

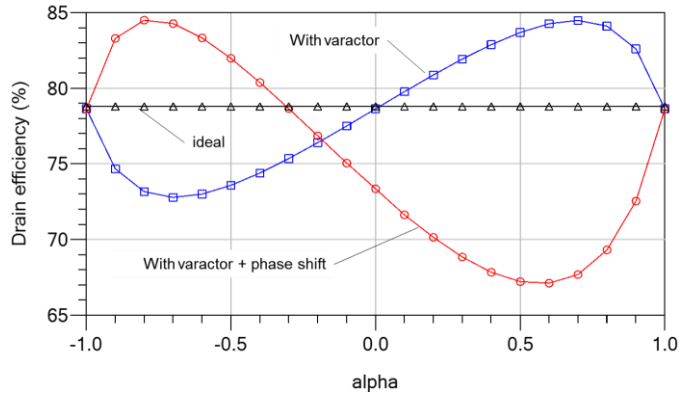


Fig. 9. Calculated output power and drain efficiency before and after phase shift.

However, for  $\alpha < -0.3$ , the calculated drain efficiency is higher than the theoretical class-B efficiency number, since the  $C_{DS}$  effect is now exploited to provide a 2<sup>nd</sup> harmonic injection effect within this range of  $\alpha$ . The highest drain efficiency achieved in this example is close to 85% at  $\alpha=-0.8$ . This presents an interesting observation, where the fundamental and 2<sup>nd</sup> harmonic are passively terminated at the die plane but the nonlinear  $C_{DS}$  causes an efficiency improvement compared to class-B.

The above analysis assumes a lossless  $C_{DS}$ . In Fig. 10, the efficiency benefit is recalculated with the addition of a  $C_{DS}$  series resistance, while other parameters are maintained as shown in Table I. Generally, the efficiency benefit is shown to reduce as  $C_{DS}$  becomes more lossy, and for the particular  $C_{DS}$  characteristic used and when  $\alpha=-0.4$ , efficiency reduces below that of ideal class-B when the series resistance exceeds 20  $\Omega$ .

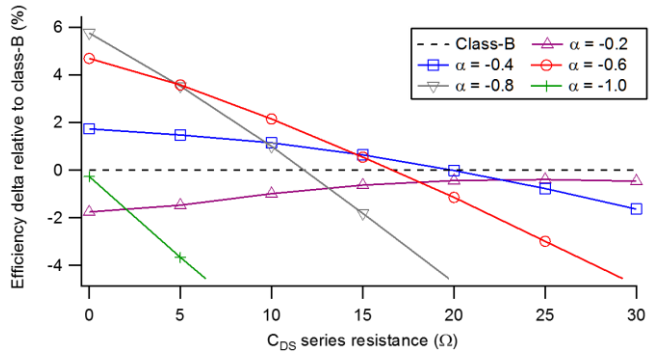


Fig. 10. Calculated effect of  $C_{DS}$  series resistance on drain efficiency.

### C. Comparison with other nonlinear $C_{DS}$ characteristics

The deviation in load trajectories and drain efficiency depends on the nonlinear characteristics of the  $C_{DS}$ . Fig. 11 compares the analysis of the  $C_{DS}$  used in section III (B) with the same analysis on two other  $C_{DS}$  shapes of different nonlinearity characteristics. The  $C_{DS}$  with  $m=1.5$  has the largest efficiency deviation as a function of  $\alpha$  since its capacitance variation is largest during the drain voltage swing.

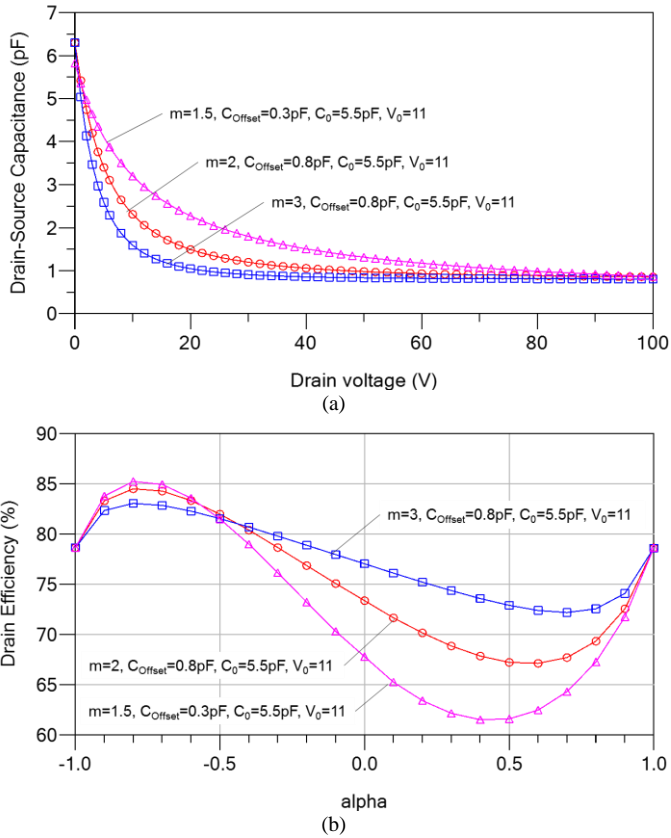


Fig. 11. Comparison of (a) three different  $C_{DS}$  shapes and (b) the corresponding drain efficiency after applying phase shift (passive 2<sup>nd</sup> harmonic terminations).

#### IV. EXPERIMENTAL VALIDATION OF THE NONLINEAR $C_{DS}$ EFFECT ON CLASS-B/J POWER AMPLIFIERS

The device under test used in this was a packaged NXP 10W, 50V LDMOS device that was drain-biased at 48V. The *Mesuro*-based active load-pull system with a Keysight PNA-X nonlinear vector network analyzer as the receiver, as described in [10] and shown in Fig. 12, was used to setup the device in a class-B operation at 900MHz. Three Keysight ESG signal generators with associated power amplifiers were used to provide the active injection on the load side to synthesize the fundamental, 2<sup>nd</sup> harmonic, and 3<sup>rd</sup> harmonic loads. A linear  $C_{DS}$  de-embedding was used to obtain the voltage and current waveforms at the device current generator plane.

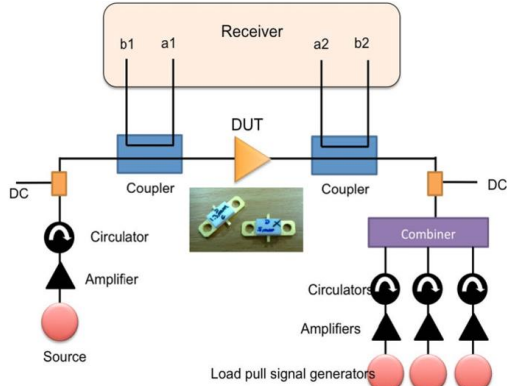


Fig. 12. Measurement setup using an active load-pull system.

The fundamental load that produced maximum efficiency ( $\sim 150 \Omega$ ) at the linear de-embedding plane was selected so that any further increase in efficiency can be attributed to the varactor's 2<sup>nd</sup> harmonic energy down-conversion. This class-B mode ( $\alpha=0$  state) was used as a reference state for the next steps.

#### A. Load-Pull Approach vs. 'Voltage-Pull' Approach

The conventional active load-pull uses target loads and iteratively changes the magnitude and phase of synthesized phase-coherent signals at the load to converge onto the target. However, to expose the varactor effect a different measurement approach is required where the desired output voltage waveform itself is set as the target at the device output. Such is the approach of this newly introduced 'voltage-pull' method, where the active load-pull system is now utilized to engineer the class-B/J voltage waveforms at the linear de-embedding plane, see Fig. 13.

Based on the measured drain current of the initial class-B load-pull setup, the required loads to produce the desired class-B/J voltage waveform were calculated for each  $\alpha$ , and entered into the active load-pull system, as shown in Fig. 14. The measured voltage waveform of the next iteration is then compared with the desired waveform, and the process is repeated until the error is minimized.

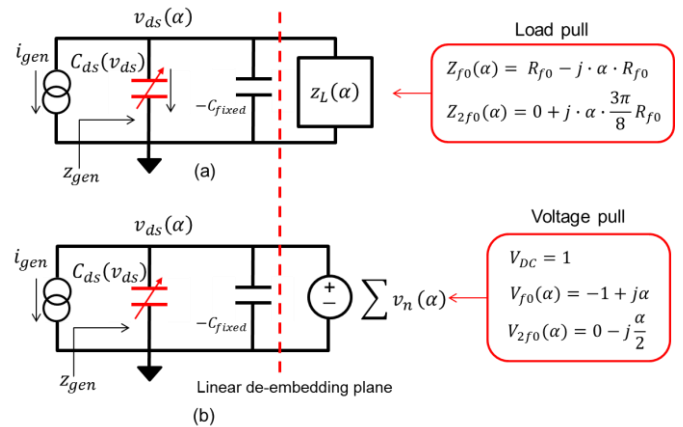


Fig. 13. Comparison of load-pull approach (a) and voltage-pull (b).

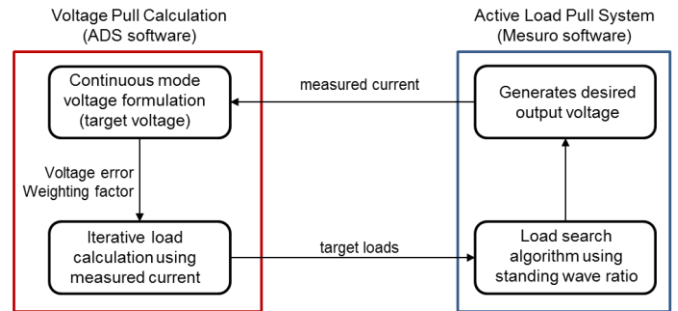


Fig. 14. Implementing voltage-pull using an active load-pull system.

The second stage in the measurement was to shift the 2<sup>nd</sup> harmonic loads to the edge of the Smith chart at the linear de-embedding plane. For this work, two methods were compared. The first method is by applying the conventional class-B/J loads

from Fig. 13(a) directly at the linear de-embedding plane. The second method is by applying a phase shift to the output voltage as in (5) in an iterative search for each  $\alpha$  such that the 2<sup>nd</sup> harmonic loads sits on the edge of the Smith chart.

### B. Voltage-Pull Measurement Results

It was observed that with the bias, load, and drive level combination, the device entered an unstable condition at  $\alpha \leq -0.6$  and  $\alpha = 1$  where the voltage-pull approach was not able to converge properly to build the desired class-B/J voltage waveforms at the output. This stability issue limited the available  $\alpha$  range for this experiment. An additional measurement point was added at  $\alpha = -0.5$  instead. Fig. 15 shows the measured voltage and current waveforms at the linear de-embedding plane for  $-0.5 \leq \alpha \leq 0.8$ , indicating a successful reconstruction of the continuous class-B/J mode of operation.

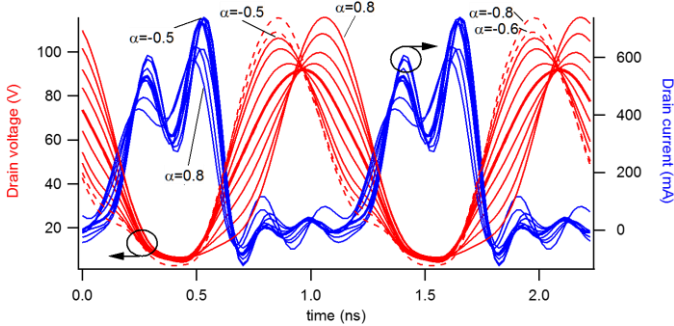


Fig. 15. Measured voltage and current waveforms at the linear de-embedding plane using voltage-pull for  $-0.5 \leq \alpha \leq 0.8$ . Expected  $\alpha = 0.6$  and  $0.8$  voltages are shown with dotted lines.

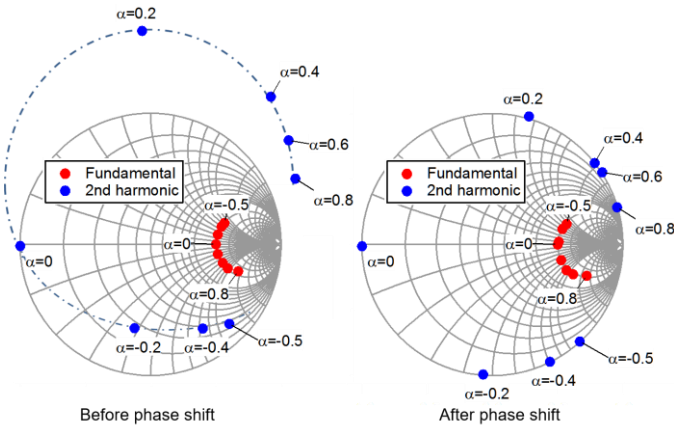


Fig. 16. Measured class-B/J fundamental and 2<sup>nd</sup> harmonic loads at the linear de-embedding plane using voltage-pull for  $-0.5 \leq \alpha \leq 0.8$  before and after phase shift.

With the device driven into compression bifurcations were present in the output current waveforms and the current peak varied with  $\alpha$  because of displacement current from the varactor. It was necessary to adjust the input drive level to have the same drain current as the  $\alpha = 0$  reference setting. For this work, the normalizing factor used when adjusting the drive level was the dc drain current instead of the maximum current ( $I_{MAX}$ ) as carried out in [11]. This was done to isolate the displacement current through  $C_{DS}$  from the ‘ideal’ current

generator, as it is assumed that the current generator current is constant for all  $\alpha$  values.

The fundamental and 2<sup>nd</sup> harmonic load trajectories for the applicable range of  $-0.5 \leq \alpha \leq 0.8$  are shown in Fig. 16. As expected from the theory, before applying the phase shift, the 2<sup>nd</sup> harmonic loads stayed inside and outside the Smith chart for the negative and positive  $\alpha$  values, respectively.

Fig. 17 shows the measured output power and drain efficiency comparison using voltage pull before and after applying phase shift. With other non-ideal factors considered such as the on-resistance, series resistance of the  $C_{DS}$ , the  $g_m$  shape of the current source, and the accuracy of the linear de-embedding used for this measurement, the efficiency curve as a function of  $\alpha$  has a different characteristic from the ideal analysis in Section III. Even the  $C_{DS}$  model itself was subject to uncertainty as a result of simplification techniques [12]. However, the trend of before and after applying the phase shift still holds.

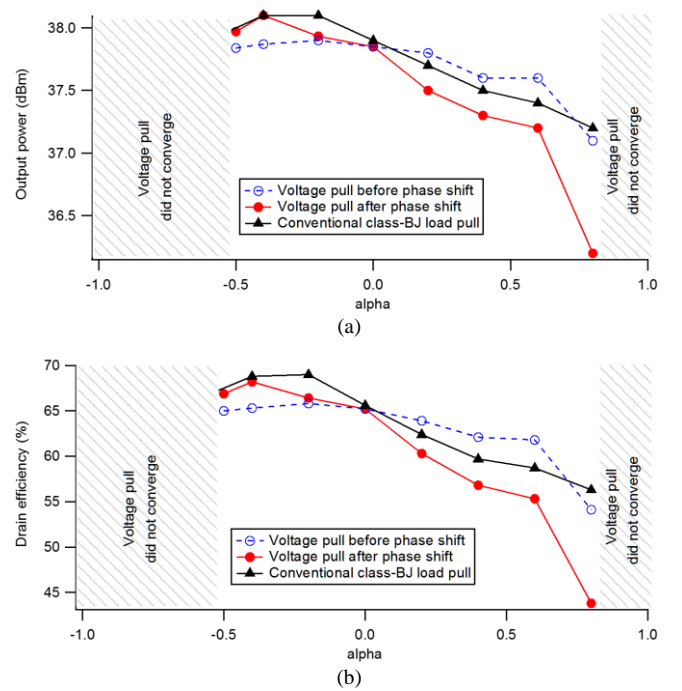


Fig. 17. Measured (a) output power and (b) drain efficiency from voltage pull before and after phase shifting, as well as from conventional class-B/J load pull.

With phase shift applied in voltage pull to bring the 2<sup>nd</sup> harmonic loads to the edge of the Smith chart, an improvement of 3%-point and 2%-point was observed at  $\alpha = -0.4$  and  $-0.5$ , respectively. This amount was small compared to prediction from the mathematical analysis which is caused by the addition of knee voltage limitation as well as a lossy element of the varactor. As expected, the drain efficiency dropped in the positive  $\alpha$  region after phase shift, due to the removal of the 2<sup>nd</sup> harmonic injection effect provided by the varactor. For this example, an interpolated phase shift was not applied to the fundamental load at  $\alpha = 0$  since the fundamental load trajectory was still approximately continuous while its corresponding 2<sup>nd</sup>

harmonic load is already at the edge of the Smith chart.

The small improvement seen at the negative  $\alpha$  region can be traced to the distribution of fundamental and 2<sup>nd</sup> harmonic power before the phase shift, as shown in Fig. 18. Before applying phase shift, the split between fundamental and 2<sup>nd</sup> harmonic power was only  $\pm 2\%$  at best, compared to 8% from the mathematical analysis where the knee voltage and  $C_{DS}$  series resistance were not considered.

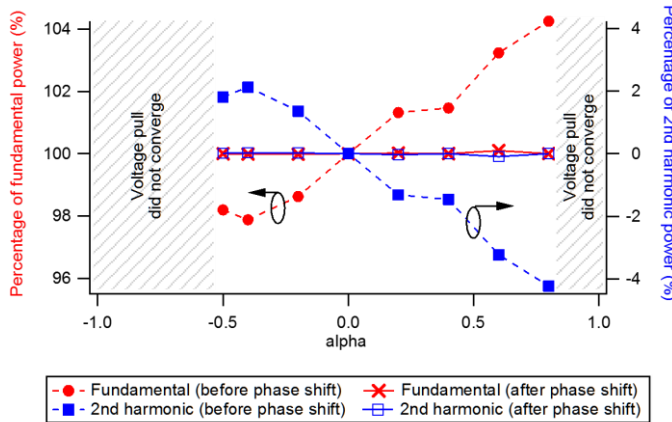


Fig. 18. Measured fundamental and 2<sup>nd</sup> harmonic power distribution.

For this device, operating condition, de-embedding selection, and  $C_{DS}$  characteristics, terminating the linear de-embedding plane with the conventional class-B/J loads produced a better efficiency overall (3.4% at  $\alpha=-0.2$  compared to class-B) but the efficiency trend across  $\alpha$  is similar to voltage pull.

## V. CONCLUSION

The nonlinear  $C_{DS}$  effect on class-B/J mode PA has been presented in this paper. It can be shown mathematically that this nonlinear effect improves the drain efficiency on one half of the continuous mode design space while degrading the other half, relative to the class-B reference mode. The mechanism behind the efficiency performance change is the energy conversion between fundamental and 2<sup>nd</sup> harmonic. In the case where efficiency is enhanced, the  $C_{DS}$  acts as a 2<sup>nd</sup> harmonic injection source, similar to the concept discussed in [4-8]. The level of efficiency improvement depends on the  $C_{DS}$ - $V_{DS}$  characteristics and series resistance.

The novel voltage-pull approach to expose the varactor effect has been introduced and experimentally validated. This method is not intended to be an alternative for load-pull in designing a PA. Rather, it provides an approach in optimizing die characteristics for transistor manufacturers, specifically in engineering the  $C_{DS}$ - $V_{DS}$  nonlinear characteristics for continuous mode applications.

## REFERENCES

- [1] S. C. Cripps, P. J. Tasker, A. L. Clarke, J. Lees, and J. Benedikt, "On the continuity of high efficiency modes in linear RF power amplifiers," *IEEE Trans. Microw. Wireless Letters Compon. Lett.*, vol. 19, no. 10, pp. 665-667, Oct. 2009.
- [2] V. Carrubba, A. L. Clarke, M. Akmal, J. Lees, J. Benedikt, P. J. Tasker, and S. C. Cripps, "The continuous class-F mode power amplifier," in *Proc. 40th Eur. Microw. Conf.*, Sep. 2010, pp. 1674-1677.
- [3] V. Carrubba, J. Lees, J. Benedikt, P. J. Tasker, and S. C. Cripps, "A novel highly efficient broadband continuous class-F RFPA delivering 74% average efficiency for an octave bandwidth," in *IEEE MTT-S Int. Microw. Symp. Dig.*, Baltimore, US, Jun. 2011, pp. 1-4.
- [4] H. Matsubara, F. Kawanabe, and T. Nojima, "A 2-GHz band experiment on efficiency enhancement of a GaN power amplifier using 2nd harmonic injection," in *Proc. Asia-Pacific Microw. Conf.*, 2008, pp. 1-4.
- [5] M. Haynes, S. C. Cripps, J. Benedikt, and P. J. Tasker, "PAE improvement using 2nd harmonic source injection at X-band," in *Proc. Works. on Integr. Nonlin. Microw. and Millimetrew. Circuits.*, 2012, pp. 1-3.
- [6] H. R. Bae, C. S. Cho, and J. W. Lee, "Efficiency enhanced class-E power amplifier using the second harmonic injection at the feedback loop," in *Proc. 40th Eur. Microw. Conf.*, Sep. 2010, pp. 1042-1045.
- [7] M. Seo, H. Lee, J. Gu, H. Kim, J. Ham, W. Choi, Y. Yun, K. K. O, and Y. Yang, "High-efficiency power amplifier using an active second-harmonic injection technique under optimized third-harmonic termination," *IEEE Trans. Circuits Syst. II, Exp. Briefs*, vol. 61, no. 8, pp. 549-553, 2014.
- [8] A. Dani, M. Roberg, and Z. Popovic, "PA efficiency and linearity enhancement using external harmonic injection," *IEEE Trans. Microw. Theory Techn.*, vol. 60, no. 12, pp. 4097-4106, Dec. 2012.
- [9] S. C. Cripps, *RF Power Amplifiers for Wireless Communications*, Artech House, 2006.
- [10] Z. Mokhtari, J. Lees, P. Tasker, and C. Cassan, "Investigating the linearity versus efficiency trade-off of different power amplifier modes in an envelope tracking architecture," in *Proc. 10th Eur. Microw. Integr. Circuits Conf.*, Sep. 2015, pp. 357-360.
- [11] V. Carrubba, "Novel highly efficient broadband continuous power amplifier modes," PhD thesis, Cardiff University, Cardiff, UK, 2012.
- [12] P. Aaen, J. A. Pl, and J. Wood, *Modeling and Characterization of RF and Microwave Power FETs*, Cambridge University Press, 2007.



**Zulhazmi A. Mokhtari** received the B.Eng. in electrical engineering and mathematics from Vanderbilt University, Nashville, TN, in 1999, and the MSc and PhD degrees from Cardiff University, UK, in 2012 and 2016, respectively, both in wireless & microwave communications. His PhD research focused on integrating high-efficiency continuous in envelope tracking architectures using waveform engineering.

From 2000 to 2008 he worked with Agilent / Keysight Technologies, Malaysia in the RF spectrum analyzers division as a manufacturing engineer and then as a new product introductions manager. He is currently an RF design engineer at Cree's Wolfspeed division, Morgan Hill, CA, in the Technology Development group.



**Jonathan Lees** received the M.Sc. and PhD. degrees in electronic engineering from Cardiff University, UK in 2002 and 2006, respectively. He is currently a Senior Lecturer with Cardiff University.

His key research areas are linear-efficient PA design and characterization with a specific interest in the design and optimization of high-efficiency power amplifiers. His work in this area culminated in the first published GaN Doherty amplifier.

His more recent research areas are the development of novel high-power, broadband time-domain measurement and load-pull techniques, as well as investigation into RF properties of materials, microwave heating, and novel applications of microwave engineering.



**Cedric Cassan** received his PhD in electrical engineering from Limoges University in 2002. Since 2002 he has been with Motorola / Freescale / NXP, in both Tempe AZ (USA) and Toulouse (France) locations, working first on RF power transistor design and then RF applications engineering, where he currently holds a Europe RF applications manager position.

His R&D interests are focused on high efficiency amplifier design (Doherty), switch mode power amplifiers, and wideband linear transmitters.

the Compound Semiconductor Centre (CSC), the CS Catapult and the EPSRC “Future Compound Semiconductor Manufacturing Hub”. He is involved in collaborative projects with a wide range of academic and industrial partners. He is a regular speaker at International conferences, and was awarded the honor of Distinguished Microwave Lecturer by the IEEE MTT society (2008 – 2010).



**Alexander Alt** received a B.Eng. degree in Information Technology from the University of Applied Science in 2011, a BEng (Hons) degree in Electrical and Electronic Engineering from the University of East London in 2012 and, in 2017, a MSc degree in Wireless & Microwave Communication Engineering from Cardiff University where he is now working towards a PhD in the Centre for High Frequency Engineering.

He was an RF R&D Engineer with TRUMPF Huettinger from 2012 to 2015. His research interests include high efficiency broadband power amplifiers, particularly envelope tracking PAs, RF power converters and device characterization and optimization.



**Paul J. Tasker** FIEEE, FIET, FLSW has over 30 years of experience in the design, fabrication, characterization and modelling of high frequency devices. From 1983-1990, he led research at Cornell, USA establishing HFETs as the technology of choice for high frequency applications. Collaboration with General Electric led to the first use of HFET technology in radio telescopes used by NRAO to receive transmissions from NASA’s Voyager 2. From 1990-95, he directed the GaAs MMIC technology development at IAF, Freiburg, Germany, delivering state-of-the-art 60-100GHz GaAs MMICs. During this period, the IAF established itself as one of Europe’s leading centers in MMIC design, fabrication and characterization. In 1995 he joined Cardiff University, establishing the center for high-frequency engineering (CHFE) in 1996. The CHFE is now recognized internationally for its pioneering work in developing waveform engineering concepts and their application to microwave and millimeter-wave power amplifier design. He was recently involved in the strategic development of the South Wales Compound Semiconductor (CS) Cluster, the establishment of